Rare Metal Materials and Engineering
Volume 51, Issue 7, July 2022
Available online at www.rmme.ac.cn

Science Press

Cite this article as: Yin Zhikun, Wang Chang, Sun Zhichao, et al. Parameter Matching of Near-β Forging+Solution and Aging Treatment for Near-α Titanium Alloy with Tri-modal Microstructure[J]. Rare Metal Materials and Engineering, 2022, 51(07): 2409-2419.

ARTICLE

Parameter Matching of Near-β Forging+Solution and Aging Treatment for Near-α Titanium Alloy with Tri-modal Microstructure

Yin Zhikun[1], Wang Chang[1,2], Sun Zhichao[1], Huang Long[1], Wang Yu[1], Yin Lijiao[1]

[1] School of Materials Science and Engineering, Northwestern Polytechnical University, Xi'an 710072, China; [2] Shaanxi Key Laboratory of Biomedical Metal Materials, Northwest Institute for Nonferrous Metal Research, Xi'an 710016, China

Abstract: Based on the orthogonal experiment results, the significance of process parameters of near-β forging+solution and aging was analyzed. The effect of process parameters on the microstructure of TA15 alloy was discussed, and the proper process parameters were obtained to achieve the tri-modal microstructure with excellent properties. Results show that the deformation temperature, solution temperature, and solution duration are the most important process parameters, which affects mostly the volume fraction and diameter of the equiaxed α_p phase, the volume fraction of the lamellar α_s phase, and the thickness of the lamellar α_s phase, respectively. The optimal processing parameters are 970 °C/0.1 s^{-1}/deformation degree of 60%/water quenching+930 °C/1.5 h/air cooling+550 °C/5 h/air cooling.

Key words: near-α titanium alloy; orthogonal experiments; near-β forging; solution and aging treatment; tri-modal microstructure

TA15 (Ti-6.5Al-2Zr-1Mo-1V) alloy is a typical near-α titanium alloy and has been widely used in the manufacture of the key load-bearing structural parts of advanced aircraft. The excellent comprehensive mechanical properties of TA15 alloy depend on its internal microstructure characteristics[1-4]. Zhou et al[5] found that titanium alloys with tri-modal microstructure, which consists of 20vol% primary equiaxed α_p phase, 50vol% ~60vol% secondary lamellar α_s phase, and transformed β matrix, can meet the service requirements. For TA15 alloy, the process of near-β forging at 10~20 °C followed by water quenching (WQ) combined with solution and aging treatment (SAT) at 40~100 °C is an effective way to obtain the tri-modal microstructure[6], and it may solve the problems of distortion and even cracking of components caused by two times of WQ, which are the disadvantages resulting from the current near-β forging process combined with high-temperature toughening and low-temperature strengthening[7].

The modified near-β forging process includes the near-β forging and subsequent SAT. The near-β forging not only affects the proportion of α and β phases as well as the morphology and distribution of equiaxed α_p phase, but also results in distortion energy rise and crystal defects which provide the nucleation sites and promote the precipitation of lamellar α_s phase during the subsequent cooling or heat treatment. Increasing the cooling rate after near-β forging leads to the changes of α_s phase from β-α transformation in the cooling process to martensitic decomposition during the subsequent solution treatment[8,9]. The formation of the trimodal microstructure and the morphology of the component phases are jointly determined by the near-β forging and SAT. The characteristics of the component phases are sensitive to the process conditions and related coupling effects[10-13]. Meanwhile, the influence of treatment processes on microstructure is heritable[14-16], which complicates the microstructure evolution, diversifies the microstructure morphologies, and impedes the controllable manufacture of tri-modal microstructure. Besides, the tri-modal microstructure has strict requirements on the volume fraction and size of the component phases. Therefore, the reasonable parameter matching

Received date: November 13, 2021
Foundation item: National Natural Science Foundation of China (52075447)
Corresponding author: Sun Zhichao, Ph. D., Professor, State Key Laboratory of Solidification Processing, School of Materials Science and Engineering, Northwestern Polytechnical University, Xi'an 710072, P. R. China, Tel: 0086-29-88460212-802, E-mail: zcsun@nwpu.edu.cn

of the near-β forging and SAT to obtain the alloy with tri-modal microstructure and excellent performance needs further investigation.

The influence of deformation and heat treatment on the microstructure of near-α titanium alloys has been widely discussed. It is found that for TA15 alloy, the volume fraction and size of equiaxed α_p phase are decreased with increasing the deformation temperature, and they are increased firstly and then decreased with increasing the deformation degree[17-19]. The strain rate also has an important influence on the microstructure morphology. Zhu et al[20] found that the thermal deformation can cause the fracture and spheroidization of strip primary α phase, and the large strain can promote the grain refinement. Yu et al[21] found that when the two-phase field of alloy is forged and then air-cooled, the aspect ratio of the lamellar α_s phase in Ti-6Al-4V alloy is decreased with increasing the deformation degree; while its volume fraction is increased with increasing the deformation degree or deformation temperature. He et al[16] revealed that after different β forging processes with a final heat treatment, different morphologies and sizes of component phases can be observed in TA15 alloy owing to the microstructure heritability. The influence of the deformation conditions on the microstructure has been widely investigated, but the effect of the subsequent heat treatment is rarely considered.

Zhu et al[22] concluded that increasing the cooling rate after $\alpha+\beta$ heat treatment can increase the growth rate of the equiaxed α_p phase in TA15 alloy. Abbasi et al[23] suggested that for Ti-6Al-4V alloy, the size of α grains increases through the static spheroidization during the subsequent heat treatment, when the strain is too small to complete the dynamic spheroidization. This phenomenon is more obvious when the temperature is 870~920 °C. Xu et al[24] indicated that with prolonging the holding time of heat treatment, the size of equiaxed α_p phase in Ti-17 alloy is increased and the static coarsening rate is reduced. Sun et al[17] demonstrated that for near-β forged TA15 alloy, the subsequent solution conditions can affect the volume fraction and morphology of equiaxed α_p and lamellar α_s phases. The main function of aging treatment is to homogenize and stabilize the alloy microstructure.

The above results indicate that the forging conditions (deformation temperature, deformation degree, strain rate) and SAT conditions (solution temperature, solution time, cooling mode, and aging temperature) dissimilarly affect the volume fraction and size of the component phases in the final alloy microstructure. However, those results cannot be directly used for the tri-model microstructure. Many thermomechanical processing parameters and microstructure characteristic parameters are involved. Thus, the orthogonal experiment was used in this research to conduct the analyses, providing an effective study of the effect of the deformation and heat treatment conditions on the final microstructure parameters.

In this research, the effects of the near-β forging and SAT on the microstructure of TA15 alloy were investigated through orthogonal experiments. The significant influence factors on the volume fraction and size of the equiaxed α_p and the lamellar α_s phases were analyzed. A reasonable parameter matching was determined to obtain the alloy with a desired tri-modal microstructure.

1 Experiment

The forged billet of TA15 alloy (Western Superconducting Technologies Co., Ltd) was used, and its chemical composition is shown in Table 1. The raw TA15 alloy was smelted thrice by a vacuum consumable electric arc furnace, and then the original billet was obtained by blanking, forging, and annealing under the condition of 820 °C/150 min/air cooling (AC). The original billet shows a typical equiaxed structure with 51.0vol% equiaxed α_p phase with average diameter of 11.0 μm and average aspect ratio of 1.71, as shown in Fig.1. The measured β-transus temperature is 985~990 °C.

The cylindrical specimens with the size of Φ10 mm×15 mm were machined from the forged billet by wire cutting, compressed at near-β temperatures by a Gleeble-3500 thermal simulator with a constant strain rate, then water quenched immediately, and finally subjected to SAT. The thermomechanical processing route is displayed in Fig.2. Subsequently, the specimens for microstructure observation were mechanically polished and etched by a solution consisting of 9vol% HF, 27vol% HNO_3, and 64vol% H_2O. The microstructure observation was conducted by OLYMPUS PMG3 optical microscope (OM). The quantitative analysis was conducted by the Image-Pro Plus 6.0 image analysis software, and the relative errors were less than 5%.

In this research, the volume fraction and diameter of the equiaxed α_p phase and the volume fraction and thickness of the lamellar α_s phase were selected as evaluation indicators of the orthogonal experiment design. The near-β deformation temperature T_1, deformation degree ε, strain rate $\dot{\varepsilon}$, solution temperature T_2, solution time t_1, solution cooling mode, and aging temperature T_3 were selected as influencing factors. The factors and levels of the near-β forging and SAT experiments are shown in Table 2. SAC indicates the slow air cooling. An orthogonal array OA_{18} (3^7) of these seven factors at different levels was employed to design the experiments, as shown in Table 3.

The mechanical properties were tested to further determine the reasonable processing parameters, and it was compared with those of alloys with the four traditional microstructures (equiaxed, bi-modal, basket-weave, and Widmanstätten microstructures). The original forged billet is regarded as the forging with equiaxed structure, and the forgings with bi-modal,

Table 1 Chemical composition of forged billet of TA15 alloy (wt%)

Al	Zr	Mo	V	Si	C	Fe	O	N	H	Ti
6.75	2.23	1.78	2.24	<0.04	<0.006	0.14	0.12	<0.002	0.002	Bal.

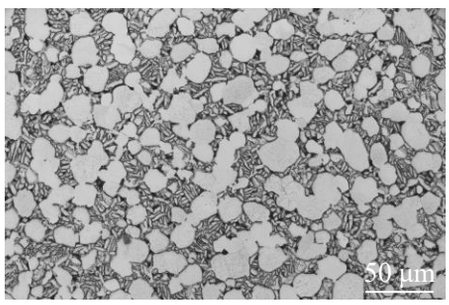

Fig.1 Original microstructure of forged billet of TA15 alloy

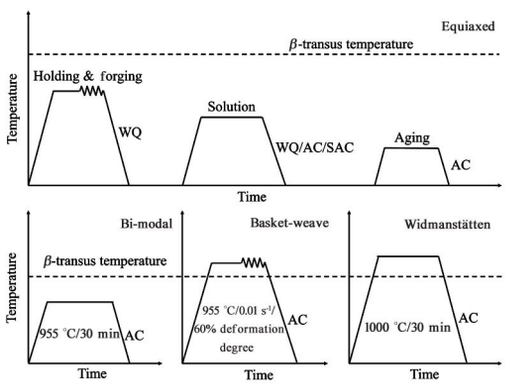

Fig.2 Schematic diagram of different thermomechanical processes for different microstructures

Table 2 Factors and levels of near-β forging and SAT experiments

Factor	Level		
	1	2	3
Deformation temperature, T_1/°C	965	970	975
Deformation degree, ε/%	20	40	60
Strain rate, $\dot{\varepsilon}/s^{-1}$	0.01	0.1	1.0
Solution temperature, T_2/°C	930	940	950
Solution cooling mode	WQ	AC	SAC
Solution time, t_1/h	0.5	1.0	1.5
Aging temperature, T_3/°C	550	600	650

basket-weave, and Widmanstätten structures were obtained by different thermomechanical processes, as shown in Fig.2.

The forgings were processed into standard tensile specimens for mechanical property tests based on the HB5143-96 and HB5195-96 standards. The mechanical property tests at room temperature and high temperature (500 ° C) were conducted on an ENST-1196 tensile testing machine, and the tensile rate was 2 mm/min. Three specimens were examined for each processing route, and the average value of the mechanical properties was used.

2 Results and Discussion

2.1 Microstructures after near-β forging and SAT

Fig. 3 shows the microstructures of TA15 alloys after the orthogonal experiments. It can be seen that all the microstructures are composed of equiaxed α_p phase, lamellar α_s phase, and transformed β matrix, but the characteristic parameters of component phases change greatly under different processing conditions. In general, the volume fraction and the size of the lamellar α_s phase are more sensitive to the processing condition than that of the equiaxed α_p phase.

The lamellar α_s phase dissolves in preference to the equiaxed α_p phase during the heating and preservation of near-β forging, namely the $\alpha \rightarrow \beta$ transformation[25]. Due to the high forging temperature, the volume fraction of equiaxed α_p phase is small, and the deformation resistance of close-packed hexagonal (hcp) α phase is higher than that of body-centered cubic (bcc) β phase during near-β forging[26,27]. Therefore, the β-phase suffers the major deformation and the deformation amount of equiaxed α_p phase is very small. The dynamic recrystallization of β phase is an important softening mechanism of near-β forging[28-31], which has an important influence on the β grains and subsequent formation of lamellar α_s phase. After WQ followed by forging, the unstable martensite is formed due to the rapid cooling, and it is decomposed into lamellar α_s phase and β matrix in subsequent solution treatment process. The lamellar α_s phase nucleates at three positions: the equiaxed α_p grain boundary, the martensite grain boundary, or the martensite interior, which is consistent with the results in Ref.[17,32]. In the whole process of near-β forging and SAT, the equiaxed α_p phase mainly undergoes the partial dissolution, nucleation with growth, Oswald ripening, and slight deformation, while the lamellar α_s phase undergoes the complete dissolution, nucleation with growth, Oswald ripening, and spheroidization. Obviously, the evolution of the lamellar α_s phase shows more significant effect on the morphology.

In this research, the lamellar α_s phase originates from the decomposition of martensite during the solution treatment, which naturally highly depends on the solution temperature. According to Fig.3c, 3h, 3l, 3p, and 3q, the lamellar α_s phase with small volume fraction at high solution temperatures of 940 and 950 ° C implies that the solution temperature has a noticeable influence on the volume fraction of the lamellar α_s phase.

2.2 Significance analysis of process parameters

The significance analysis of each process parameter for their effect on the volume fraction and size of α phase was conducted. The range analysis method was adopted. Thus, two parameters of K_{ij} and R_j were calculated, where K_{ij} is the sum of the experiment results of the evaluation indicator j (the volume fraction of equiaxed α_p phase-V_1, the average diameter of equiaxed α_p phase-d_1, the volume fraction of lamellar α_s phase-V_2, and the thickness of lamellar α_s phase-d_2) under the corresponding factor of the level i, reflecting the dependence of the indicator on the factor, and R_j is the range of K_{ij}, reflecting the significance of the factor on the evaluation indicator j. The larger the range, the more important the factor for the indicator, which is generally considered as the main factor affecting the indicator. Conversely, a small range

Table 3 Results and analyses of orthogonal experiments

No.	T_1/°C	ε/%	$\dot{\varepsilon}$/s^{-1}	T_2/°C	Solution cooling mode	t_1/h	T_3/°C	Phase content/vol%		Diameter of equiaxed α_p phase, d_1/μm	Thickness of secondary lamellar α_s phase, d_2/μm
								Equiaxed α_p phase, V_1	Secondary lamellar, α_s phase, V_2		
1	965	20	0.01	930	WQ	0.5	550	21.43	24.51	8.61	0.96
2	965	40	0.1	940	AC	1.0	600	20.21	29.13	7.31	1.26
3	965	60	1.0	950	SAC	1.5	650	18.04	15.71	6.72	1.39
4	970	20	0.01	940	AC	1.5	650	15.14	29.08	7.13	1.3
5	970	40	0.1	950	SAC	0.5	550	12.91	27.85	6.67	1.26
6	970	60	1.0	930	WQ	1.0	600	17.56	28.80	7.87	1.09
7	975	20	0.1	930	SAC	1.0	650	14.28	31.08	8.76	1.02
8	975	40	1.0	940	WQ	1.5	550	15.67	18.07	8.93	0.93
9	975	60	0.01	950	AC	0.5	600	13.83	25.68	7.15	1.28
10	965	20	1.0	950	AC	1.0	550	21.61	21.05	8.77	1.06
11	965	40	0.01	930	SAC	1.5	600	20.11	40.19	8.34	1.44
12	965	60	0.1	940	WQ	0.5	650	17.98	18.43	7.27	1.14
13	970	20	0.1	950	WQ	1.5	600	13.24	36.27	7.45	1.41
14	970	40	1.0	930	AC	0.5	650	18.90	29.2	7.72	1.01
15	970	60	0.01	940	SAC	1.0	550	16.06	37.14	7.94	1.25
16	975	20	1.0	940	SAC	0.5	600	17.43	18.84	8.51	0.95
17	975	40	0.01	950	WQ	1.0	650	14.92	12.53	8.41	0.93
18	975	60	0.1	930	AC	1.5	550	13.78	39.57	7.73	1.39

usually means that the factor has little influence on the indicator.

Experiments were arranged according to the orthogonal scheme in Table 3, and the results are shown in Table 4. The volume fractions and sizes of equiaxed α_p and lamellar α_s phases are obtained under all conditions, as shown in Table 3. The significance analysis can be employed to quantitatively compare the dependence degree of the microstructure parameters on the process parameters. The range values R_1~R_4 of different factors for the volume fraction of equiaxed α_p phase (V_1), volume fraction of lamellar α_s phase (V_2), diameter of equiaxed α_p phase (d_1), and the thickness of lamellar α_s phase (d_2) are shown in Table 4, respectively. The significance orders and regularities of the factors affecting the evaluation indicators can be obtained as follows.

According to the range values of R_1, the significance order of the factors affecting the V_1 value is T_1>$\dot{\varepsilon}$>T_2>t_1>ε>solution cooling mode>T_3. The volume fraction of the equiaxed α_p phase is highly dependent on the forging temperature and it is decreased rapidly with increasing the forging temperature.

According to the range values of R_2, the significance order of the factors affecting the V_2 value is T_2>$\dot{\varepsilon}$>T_3 >T_1>solution cooling mode>t_1>ε. Except for the deformation degree ε, all the factors show significant effects on the volume fraction of the lamellar α_s phase, and the solution temperature plays the most important role. The volume fraction of lamellar α_s phase is sharply decreased with increasing the solution temperature.

According to the range values of R_3, the significance order of the factors affecting the average diameter d_1 of the equiaxed α_p phase is T_1> ε >T_2>$\dot{\varepsilon}$>t_1>solution cooling mode>T_3. The influence degrees of the forging temperature T_1 and the deformation degree ε are similar and are both significant. The average diameter of the equiaxed α_p phase is decreased firstly and then increased with increasing the forging temperature, and it is decreased rapidly with increasing the deformation degree.

According to the range values of R_4, the significance order of the factors affecting the thickness d_2 of the lamellar α_s phase is t_1>$\dot{\varepsilon}$>solution cooling mode> ε >T_1>T_3>T_2. The solution holding time t_1 has the greatest influence on d_2. The thickness of the lamellar α_s phase is increased rapidly with prolonging the solution holding time.

Consequently, the volume fraction and diameter of the equiaxed α_p phase, the volume fraction of the lamellar α_s phase, and the thickness of the lamellar α_s phase are mainly affected by the deformation temperature T_1, the solution temperature T_2, and the solution holding time t_1, respectively.

2.3 Reasonable matching and effect of representative process parameters

The orthogonal experiment design can be used not only to analyze the significance of process parameters, but also to explore the reasonable matching for the parameters. In this research, V_1, d_1, V_2, and d_2 of the final microstructure are considered as the evaluation indicators to determine the

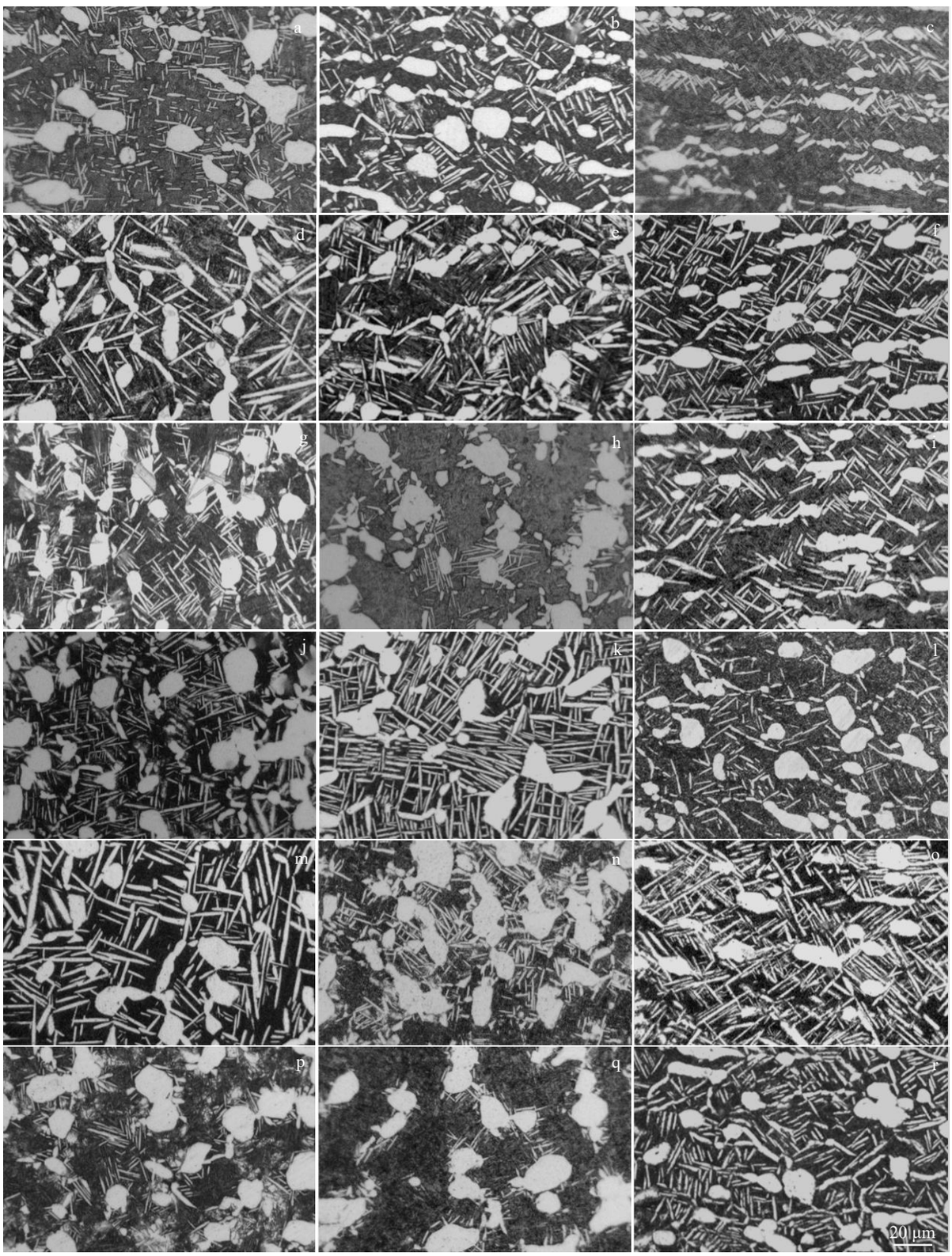

Fig.3 Microstructures of TA15 alloys after No.1~18 orthogonal experiments (a~r)

feasible ranges of the process parameters. According to the relationship between the microstructure parameters and mechanical properties in Ref.[2,5,33,34], the desired ranges of V_1, V_2, d_1, and d_2 are set as 15%~20%, 25%~60%, 7~9 μm, and 1~1.5 μm, respectively. It is found that the microstructure with 20vol% equiaxed α_p phase has a good combination of strength, ductility, and fracture toughness[2,5,34]. The microstructure with small equiaxed α_p phase and long, thick, lamellar α_s phase possesses good tensile strength, plasticity, impact toughness, and fracture toughness[33]. More and thicker

Table 4 Significance analysis results of process parameters for their effects on volume fraction and size of α phases

Factor	T_1	ε	$\dot{\varepsilon}$	T_2	Solution cooling mode	t_1	T_3
K_{11}	119.38	103.13	101.49	106	100.8	102.5	101.5
K_{21}	93.81	102.72	92.4	102	103.47	104.6	102.4
K_{31}	89.91	97.25	109.21	94.6	98.83	95.98	99.26
R_1	29.47	5.88	16.81	11.40	4.64	8.62	3.14
K_{12}	149.02	160.83	169.13	193.35	138.61	144.51	168.19
K_{22}	188.34	156.97	182.33	150.69	173.71	159.73	178.91
K_{32}	145.77	165.33	131.67	139.09	170.81	178.89	136.03
R_2	42.57	8.36	50.66	54.26	35.10	34.38	42.88
K_{13}	47.02	49.23	47.58	49	48.54	45.93	48.65
K_{23}	44.78	47.38	45.19	47.1	45.81	49.06	46.63
K_{33}	49.49	44.68	48.52	45.2	46.94	46.3	46.01
R_3	4.71	4.55	3.33	3.80	2.73	3.13	2.64
K_{14}	7.25	6.7	7.16	6.91	6.46	6.6	6.85
K_{24}	7.32	6.83	7.48	6.83	7.3	6.61	7.43
K_{34}	6.5	7.54	6.43	7.33	7.31	7.86	6.79
R_4	0.82	0.84	1.05	0.50	0.85	1.26	0.64

lamellar α_s phases can lead to higher strength and impact toughness at room temperature and high temperatures[17]. Therefore, more and finer equiaxed α_p phase as well as more and thicker lamellar α_s phase is preferred in their target ranges.

Based on the significance analyses, the relationships between indicators and those significant factors are presented in Fig. 4. According to Table 3, Table 4, and Fig. 4, it can be seen that the experiment results can generally meet the requirements of every single evaluation indicator, and the Specimen 4, 6, 14, and 15 can meet the requirements of all

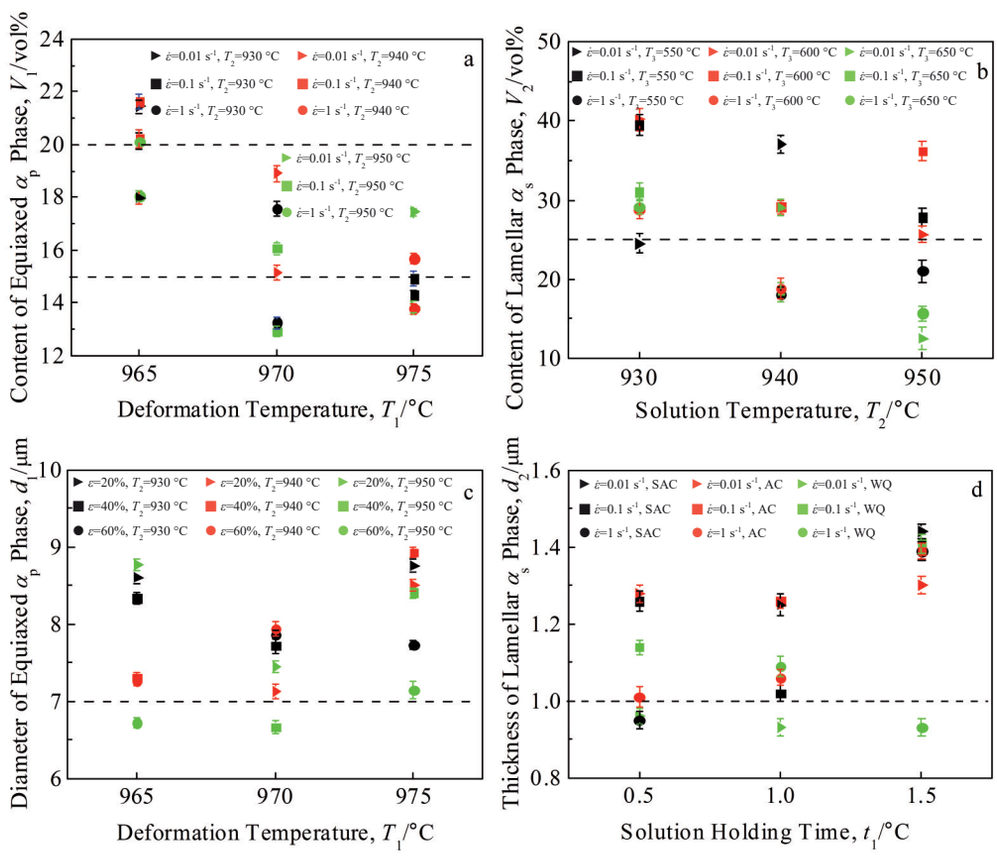

Fig.4 Relationships of volume fraction of equiaxed α_p phase V_1 (a), volume fraction of lamellar α_s phase V_2 (b), diameter of equiaxed α_p phase d_1 (c), and thickness of lamellar α_s phase d_2 (d) with different factors

indicators. The ranges of involved process parameters are as follows: deformation temperature of 970 °C, deformation degree of 20%~60%, strain rate of 0.01~1 s^{-1}, solution temperature of 930~940 °C, solution holding time of 0.5~1.5 h, solution cooling mode of AC, SAC, and WQ, and aging temperature of 550~650 °C.

Based on the K_{i3} values in Table 3, the diameter of the equiaxed α_p phase is decreased with increasing the deformation degree. Therefore, the deformation degree of 60% is more suitable. Similarly, it can be proved that the process parameters of $\dot{\varepsilon}$=0.1 s^{-1}, T_2=930 °C, t_1=1.5 h, AC, and T_3=550 °C are more appropriate.

The deformation temperature is the most important factor affecting the volume fraction and diameter of the equiaxed α_p phase, but its influence on the lamellar α_s phase is relatively weak. The lamellar α_s phase dissolves preferentially during the $\alpha \rightarrow \beta$ phase transformation[25], and the near-β forging temperature is close to the β-transus temperature. Therefore, under normal circumstances, the initial lamellar α_s phase can completely dissolve before deformation, and the change of deformation temperature cannot cause a noticeable impact on the lamellar α_s phase. The deformation degree has the second-obvious effect on the diameter of equiaxed α_p phase. Increasing the deformation degree can significantly promote the generation of deformation heat, increase the deformation temperature, strengthen the $\alpha \rightarrow \beta$ phase transformation, and further reduce the size of the equiaxed α_p phase. Since there are a few equiaxed α_p phases near the β-transus temperature and the deformation resistance of the hcp α phase is greater than that of the bcc β matrix, the equiaxed α_p phase undergoes a slight deformation[26,27]. It is unlikely to change the size of the equiaxed α_p phase through dynamic recrystallization or decomposition. The strain rate has a significant effect on both the equiaxed α_p and the lamellar α_s phases. Changes in the strain rate can significantly affect the deformation temperature[35], therefore influencing the volume fraction of the equiaxed α_p phase. It can be seen that the size of the equiaxed α_p phase is less temperature-dependent. Meanwhile, increasing the strain rate can shorten the deformation duration and inhibit the dynamic recovery and dynamic recrystallization in the high-temperature β phase. More crystal defects and distortion energy are retained, which affect the subsequent decomposition of martensite into lamellar α_s phase.

In terms of heat treatment, the solution temperature is the most important factor affecting the volume fraction of lamellar α_s phase. The lamellar α_s phase is produced by the decomposition of martensite in the solution process, and then it partially dissolves whereas the rest grows[25]. According to the phase equilibrium, the solution temperature directly affects the dissolution degree of lamellar α_s phase, i.e., the solution temperature plays a decisive role in the volume fraction of the final lamellar α_s phase. The growth of lamellar α_s phase is a long-term process, so the solution time becomes the most important factor affecting the thickness of the lamellar α_s phase. The solution cooling mode has little effect on the component phases. The evolution of the equiaxed α_p and lamellar α_s phases is basically completed before cooling[17]. The period of cooling process is shorter than that of heat preservation, so the $\beta \rightarrow \alpha$ phase transformation has little effect on component phases. Generally, the effect of aging temperature is minimal. The temperature is low and the atomic diffusion ability is very weak, so the aging treatment has little effect on the microstructure and mainly plays a role as the microstructure stabilizer[17,25]. The above analysis indicates that the deformation temperature, the solution temperature, and the solution time are all important process parameters.

2.3.1 Deformation temperature

Fig. 5 and Fig. 6 show the final microstructures and related quantitative results of TA15 alloys at deformation temperatures of 965~975 °C, respectively. Other process parameters are fixed as 930 °C/1 h/AC+550 °C/5 h/AC. With increasing the deformation temperature, the volume fraction and diameter of the equiaxed α_p phase are decreased gradually, which is mainly caused by the $\alpha \rightarrow \beta$ phase transformation. Besides, the change in the diameter is not as obvious as that in the volume fraction due to the Oswald ripening. Meanwhile, the amount of deformed equiaxed α_p phase is small. It can be seen from Fig. 5 that the equiaxed α_p phase boundary is smooth, indicating that the dynamic recrystallization can hardly occur in the equiaxed α_p phase during near-β forging. In addition, the TA15 alloy is slightly elongated due to a small amount of deformation. During the deformation at lower temperature, the initial lamellar α_s phase may not completely dissolve, and dynamic spheroidization occurs[36,37].

Meanwhile, the volume fraction and thickness of the lamellar α_s phase are increased firstly and then decreased. In

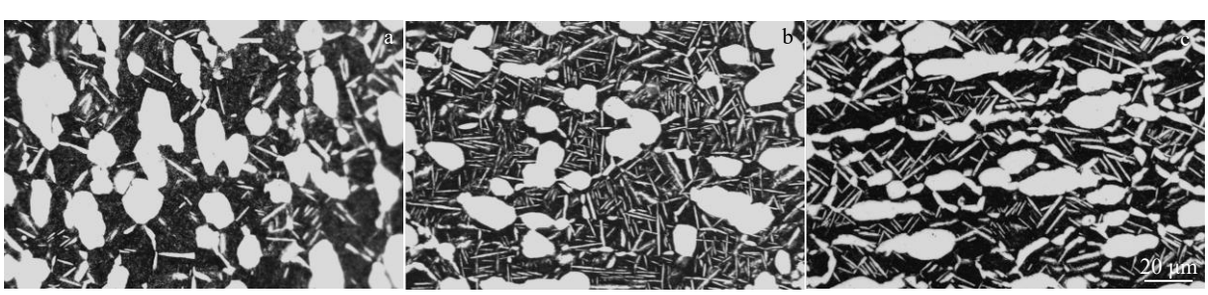

Fig.5 Final microstructures of TA15 alloys after processes of T_1/0.1 s^{-1}/60%/WQ+930 °C/1 h/AC+550 °C/5 h/AC at different deformation temperatures: (a) T_1=965 °C, (b) T_1=970 °C, and (c) T_1=975 °C

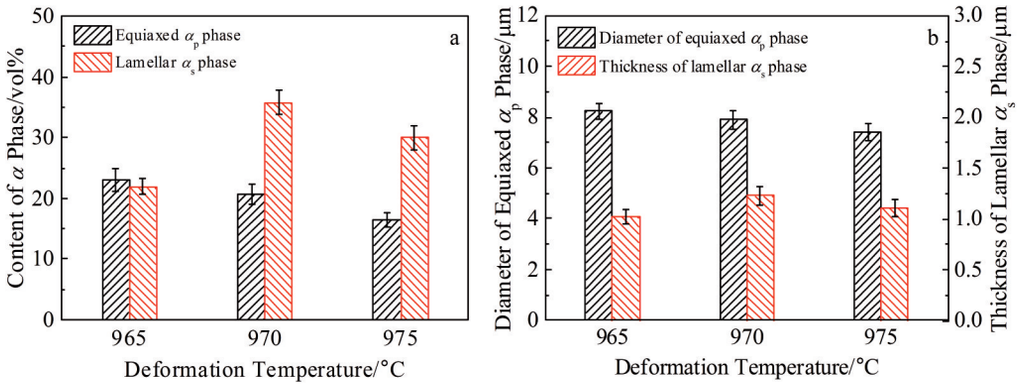

Fig.6 Volume fraction (a) and diameter/thickness (b) of α phases at different deformation temperatures

general, more martensite α' phases are generated from the high-temperature β matrix when TA15 alloy is forged at higher temperatures and then rapidly cooled by WQ, because the equiaxed α_p phase is less and the martensite is decomposed into more and thicker lamellar α_s phases in the subsequent solution process. Besides, the strengthened dynamic recovery can consume partial crystal defects and distortional strain energy[38], thereby further resulting in fewer nuclei of lamellar α_s phases. Consequently, the volume fraction and thickness of the lamellar α_s phase are increased firstly and then decreased with increasing the forging temperature.

2.3.2 Solution temperature

Fig. 7 and Fig. 8 show the final microstructures and related quantitative results of TA15 alloys at solution temperatures of 930, 940, 950 °C. The forging and aging processes are fixed as 970 °C/0.1 s^{-1}/60%/WQ and 550 °C/5 h/AC, respectively. With increasing the solution temperature, the volume fraction and diameter of the equiaxed α_p phase are decreased slightly,

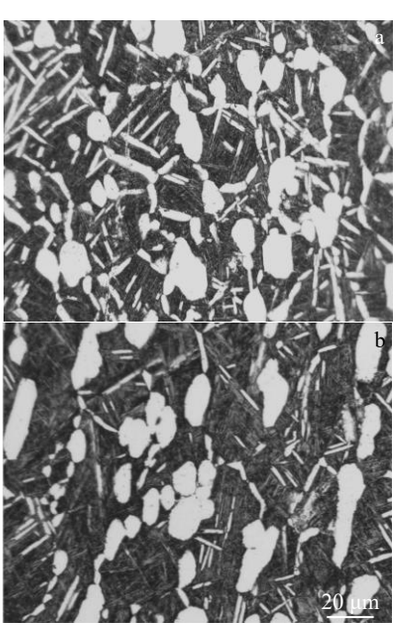

Fig.7 Final microstructures of TA15 alloys after processes of 970 °C/0.1 s^{-1}/60%/WQ+T_2/1 h/AC+550 ° C/5 h/AC at different solution temperatures: (a) T_2=940 °C and (b) T_2=950 °C

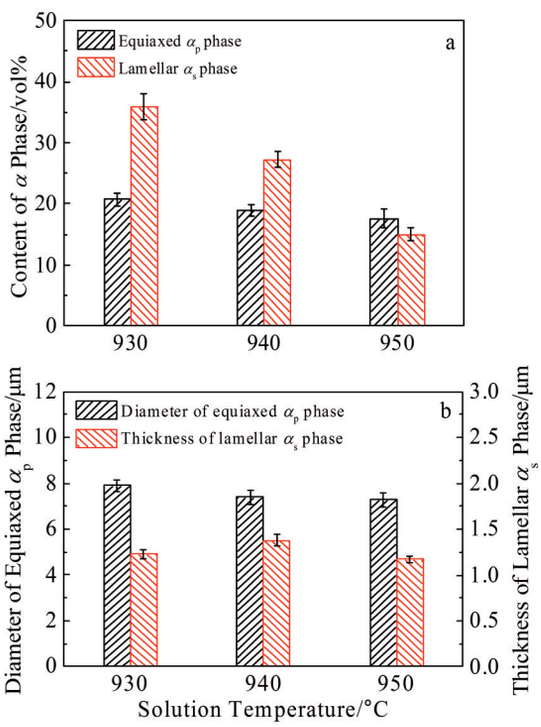

Fig.8 Volume fraction (a) and diameter/thickness (b) of α phases at different solution temperatures

while the volume fraction and thickness of the lamellar α_s phase are decreased significantly. This is due to the obvious $\alpha \rightarrow \beta$ phase transformation near the β-transus temperature[39], and the lamellar α_s phase changes before the equiaxed α_p phase. It is noteworthy that the thickness of the lamellar α_s phase is increased firstly and then decreased with increasing the solution temperature, indicating that the decomposition of martensite α' and the $\alpha \rightarrow \beta$ phase transformation occur simultaneously and they are competed with each other during the solution period.

Additionally, the Widmanstätten α phase is precipitated from the high-temperature β matrix in the cooling process[40-43]. There are three nucleation positions: α/β boundary, β/β boundary, and original β interior. From the perspective of phase equilibrium, the volume fraction of α phase and β

matrix is determined by the solution temperaturedue and the content of α and β stable elements in the alloys. Therefore, when the equiaxed α_p and lamellar α_s phases are decreased, the Widmanstätten α phase is increased. It is also found that some lamellar α_s grains nucleate and grow on the boundary of the equiaxed α_p phase.

2.3.3 Solution time

Fig.9 and Fig.10 show the final microstructures and related quantitative results of TA15 alloys after treatment for different solution durations from 0.5 h to 3 h, respectively. The deformation and aging treatment is fixed as 970 °C/0.1 s^{-1}/60%/WQ and 550 °C/5 h/AC, respectively. With prolonging the solution time, the volume fraction of the lamellar α_s phase is decreased significantly, its thickness is increased, and its distribution is more uniform, which is consistent with the results in Ref.[44]. This is because the lamellar α_s phase originates from the decomposition of the martensite α' phase during the heating and early holding period of the solution treatment, then it dissolves due to the $\alpha \rightarrow \beta$ transformation, and finally it is coarsened due to the Oswald ripening. Meanwhile, the volume fraction and diameter of equiaxed α_p phase are increased slightly with prolong the solution time, indicating that when the solution temperature is below the forging temperature, the $\beta \rightarrow \alpha_p$ transformation occurs simultaneously with the $\alpha_s \rightarrow \beta$ transformation in the solution treatment process.

3 Microstructure and Mechanical Properties Verification of Reasonable Parameter Matching

According to the obtained matching of the processing parameters, the process route of 970 °C/0.1 s^{-1}/60%/WQ+930 °C/1.5 h/AC+550 °C/5 h/AC is optimal to obtain the target tri-modal microstructure of TA15 alloy, as shown in Fig. 11a. The corresponding measured mechanical properties of TA15 alloy are shown in Table 5. The content of the equiaxed α_p phase is 18.7vol%, the average diameter of the equiaxed α_p phase is 8.2 μm, the content of the lamellar α_s phase is 36.8vol%, and the thickness of the lamellar α_s phase is 1.39 μm, which all meet the requirements of component phases in the alloys with tri-modal microstructure. According to Table 5, at room temperature, the tensile strength σ_m, yield strength $\sigma_{0.2}$, elongation A, and reduction of cross-section area Z are 990.0 MPa, 930.0 MPa, 20.0%, and 43.2%, respectively. The tensile strength σ_{mh} at 500 °C is 680.0 MPa. The impact toughness α_{ku} and fracture toughness K_{1C} are 45.0 $J \cdot cm^{-2}$ and 91.2 $MPa \cdot m^{1/2}$, respectively. All the measured mechanical properties met the requirements of the aviation forgings ($\sigma_m \geqslant$ 930 MPa, $A \geqslant 10\%$, $Z \geqslant 25\%$, $\sigma_{mh} \geqslant 630$ MPa, $\alpha_{ku} \geqslant 40$ $J \cdot cm^{-2}$)[17,33].

Metallographic photos of forgings with four traditional microstructures (equiaxed, bi-modal, basket-weave and Widmanstätten) are shown in Fig. 1 and Fig. 11b~11d, respectively. In addition, the tensile properties of the forgings were measured and listed in Table 5 in order to clearly propose the optimum processing parameters. The forging with the tri-modal microstructure does not show the best results in many indicators but has the optimal comprehensive properties. This indicates that the method and results of processing parameter matching for tri-modal microstructure are of significance.

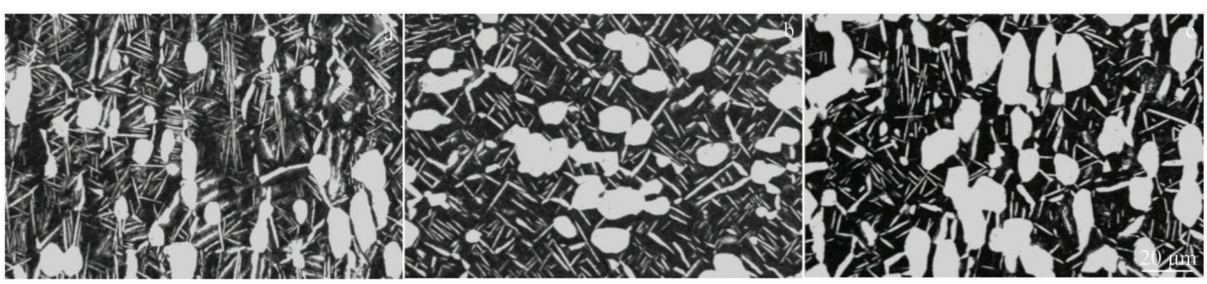

Fig.9 Final microstructures of TA15 alloys after processes of 970 °C/0.1 s^{-1}/60%/WQ+930 °C/t_1/AC+550 °C/5 h/AC for different solution durations: (a) t_1=0.5 h, (b) t_1=2 h, and (c) t_1=3 h

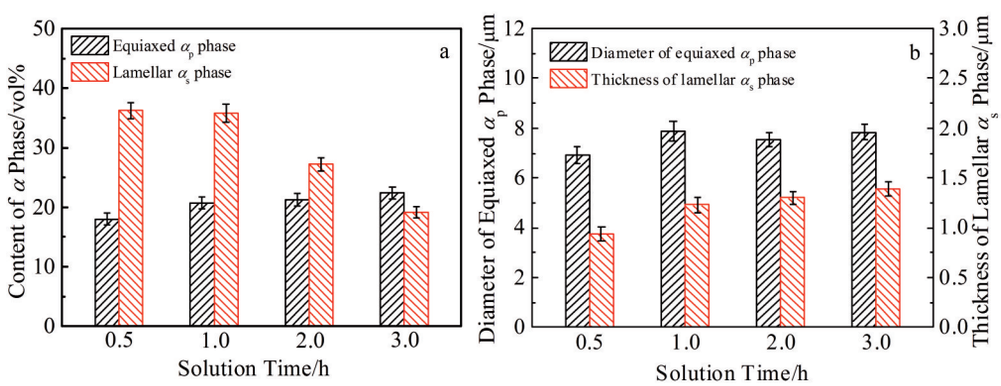

Fig.10 Volume fraction (a) and diameter/thickness (b) of α phases after processes for different solution durations

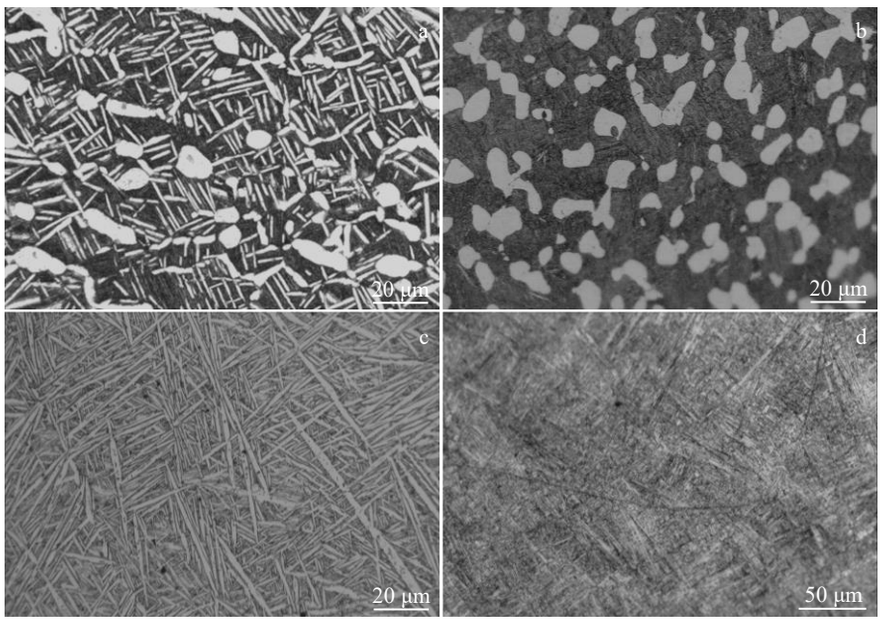

Fig.11 Tri-modal (a), bi-modal (b), Basket-weave (c), and Widmanstätten (d) microstructures of TA15 alloys

Table 5 Measured mechanical properties of TA15 alloys with different microstructures

Microstructure	V_1/vol%	V_2/vol%	d_1/μm	d_2/μm	σ_m/MPa	$\sigma_{0.2}$/MPa	A/%	Z/%	σ_{mh}/MPa
Tri-modal	18.7	36.8	8.2	1.39	990.0	930.0	20.0	43.2	680.0
Equiaxed	62.8	-	18.4	-	979.0	906.0	22.1	48.7	662.0
Bi-modal	32.7	-	7.9	-	982.0	915.0	20.6	49.4	670.0
Basket-weave	-	76.8	-	1.66	1007.0	953.0	18.2	37.3	675.0
Widmanstätten	-	79.6	-	1.17	966.0	886.0	12.2	18.6	621.0

Note: σ_m, $\sigma_{0.2}$, A, and Z are obtained at room temperature; σ_{mh} is obtained at 500 °C

4 Conclusions

1) In the process of the near-β forging and the solution and aging treatment (SAT), the deformation temperature, the solution temperature, and the solution time are the three most important process parameters, showing great effects on the volume fraction and diameter of the equiaxed α_p phase, the volume fraction of the lamellar α_s phase, and the thickness of the lamellar α_s phase, respectively.

2) The optimal process parameters are as follows: the deformation temperature is 970 °C, the deformation degree is 60%, the strain rate is 0.1 s^{-1}, the solution temperature is 930 °C, the solution holding time is 1.5 h, the solution cooling mode is air cooling, and the aging temperature is 550 °C.

3) The tri-modal microstructure of TA15 alloy with excellent performance can be obtained, indicating that the parameter matching method in this research is of significance in production design.

References

1 Fan X G, Yang H, Gao P F. *Materials and Design*[J], 2013, 51: 34

2 Gao P F, Qin G, Wang X X *et al*. *Materials Science and Engineering A*[J], 2019, 739: 203

3 Banerjee D, Williams J C. *Acta Materialia*[J], 2013, 61(3): 844

4 Semiatin S L. *Metallurgical and Materials Transactions A*[J], 2020, 51(6): 2593

5 Zhou Y G, Zeng W D, Yu H Q. *Materials Science and Engineering A*[J], 2005, 393(1-2): 204

6 Sun Z C, Liu L, Yang H. *Materials Science and Engineering A* [J], 2011, 528(15): 5112

7 Zhou Y G, Zeng W D, Yu H Q. *Materials Science and Engineering A*[J], 1996, 221(1-2): 58

8 Stanford N, Bate P S. *Acta Materialia*[J], 2004, 52(17): 5215

9 Malinov S, Guo Z, Sha W *et al*. *Metallurgical and Materials Transactions A*[J], 2001, 32(4): 879

10 Meng M, Fan X G, Yang H *et al*. *Journal of Alloys and Compounds*[J], 2017, 714: 294

11 Gao X X, Zeng W D, Zhang S F *et al*. *Acta Materialia*[J], 2017, 122: 298

12 Ouyang D L, Cui X, Lu S Q *et al*. *Journal of Materials Research and Technology*[J], 2020, 9(6): 15 662

13 Zhang L C, Chen L Y. *Advanced Engineering Materials*[J], 2019, 21(4): 1 801 215

14 Lei Z N, Gao P F, Li H W *et al*. *Materials Characterization*[J],

2017, 134: 236
15 Hou Zhimin, Mao Xiaonan, Lei Wenguang *et al*. *The Chinese Journal of Nonferrous Metals*[J], 2010, 20(Z1): 604 (in Chinese)
16 He D, Zhu J C, Zaefferer S *et al*. *Materials Science and Engineering A*[J], 2012, 549: 20
17 Sun Z C, Mao X J, Wu H L *et al*. *Materials Science and Engineering A*[J], 2016, 654: 113
18 Seshacharyulu T, Dutta B. *Scripta Materialia*[J], 2002, 46(9): 673
19 Momeni A, Abbasi S M. *Materials and Design*[J], 2010, 31(8): 3599
20 Zhu J C, Wang Y, Liu Y *et al*. *Transactions of Nonferrous Metals Society of China*[J], 2007, 17(S1): 490
21 Yu W X, Li M Q, Luo J. *Materials Science and Engineering A* [J], 2010, 527(16-17): 4210
22 Zhu S, Yang H, Guo L G *et al*. *Materials Characterization*[J], 2012, 70: 101
23 Abbasi S M, Momeni A. *Transactions of Nonferrous Metals Society of China*[J], 2011, 21(8): 1728
24 Xu J W, Zeng W D, Jia Z Q *et al*. *Journal of Alloys and Compounds*[J], 2015, 618: 343
25 Wu H L, Sun Z C, Cao J *et al*. *Journal of Alloys and Compounds* [J], 2019, 786: 894
26 Shi X H, Zhao C, Cao Z H *et al*. *Progress in Natural Science: Materials International*[J], 2019, 29(4): 432
27 Fan X G, Jiang X Q, Zeng X *et al*. *International Journal of Plasticity*[J], 2018, 104: 173
28 Liu H J, Zhang Z M, Xu K H *et al*. *Materials Characterization* [J], 2021, 178: 111 263
29 Jiang X Q, Fan X G, Zhan M *et al*. *Materials and Design*[J], 2021, 203: 109 589
30 Lei J, Zhu W G, Chen L *et al*. *Materials Today Communications* [J], 2020, 23: 100 873
31 Warchomicka F, Poletti C, Stockinger M. *Materials Science and Engineering A*[J], 2011, 528(28): 8277
32 Sun Z C, Han F X, Wu H L *et al*. *Journal of Materials Processing Technology*[J], 2016, 229: 72
33 Sun Z C, Wu H L, Sun Q F *et al*. *Materials Characterization*[J], 2016, 121: 213
34 Lütjering G. *Materials Science and Engineering A*[J], 1998, 243(1-2): 32
35 Xu J W, Zeng W D, Zhao Q Y *et al*. *Materials Science and Engineering A*[J], 2021, 803: 140 723
36 Semiatin S L, Stefansson N, Doherty R D. *Metallurgical and Materials Transactions A*[J], 2005, 36(5): 1372
37 Sun Z C, Yin Z K, Cao J *et al*. *JOM*[J], 2019, 71(12): 4746
38 Wu C, Yang H, Li H W. *Journal of Materials Processing Technology*[J], 2013, 213(11): 2033
39 Wang T, Guo H Z, Tan L J *et al*. *Materials Science and Engineering A*[J], 2011, 528(21): 6375
40 Bhattacharyya D, Viswanathan G B, Fraser H L. *Acta Materialia* [J], 2007, 55(20): 6765
41 Zhang J, Li H W, Sun X X *et al*. *International Journal of Plasticity*[J], 2020, 135: 102 804
42 Lu Z M, Luo J, Wang B Z *et al*. *Materials and Design*[J], 2020, 189: 108 490
43 Ji X K, Guo B Q, Jiang F L *et al*. *Journal of Materials Science and Technology*[J], 2020, 36: 160
44 Zhu Jingchuan, He Dong, Yang Xiawei *et al*. *Rare Metal Materials and Engineering*[J], 2013, 42(2): 382 (in Chinese)

基于三态组织的近α钛合金近β锻+固溶时效工艺参数匹配

印志坤[1]，王　昌[1,2]，孙志超[1]，黄　龙[1]，王　钰[1]，尹丽娇[1]
(1. 西北工业大学 材料学院，陕西 西安 710072)
(2. 西北有色金属研究院 陕西省医用金属材料重点实验室，陕西 西安 710016)

摘　要：基于正交试验结果，对近β锻+固溶时效工艺参数进行了显著性分析，并详细讨论了工艺参数对TA15钛合金显微组织的影响及合理的工艺参数，以获得性能优异的三态组织。结果表明：变形温度、固溶温度和固溶时间是3个最为重要的工艺参数，分别对等轴α_p相的体积分数和直径、片层α_s相的体积分数及片层α_s相的厚度影响最大。较合理的TA15钛合金处理工艺参数为970 ℃/0.1 s^{-1}/60%变形程度/水淬+930 ℃/1.5 h/空冷+550 ℃/5 h/空冷。

关键词：近α钛合金；正交实验；近β锻造；固溶时效处理；三态组织

作者简介：印志坤，男，1994年生，博士生，西北工业大学材料学院凝固技术国家重点实验室，陕西 西安 710072，电话：029-88460212-802，E-mail：zhikunyin@163.com